Simultaneous Geometric - Iconic Registration

Aristeidis Sotiras[1,2], Yangming Ou[3],
Ben Glocker[4], Christos Davatzikos[3], and Nikos Paragios[1,2]

[1] Laboratoire MAS, Ecole Centrale de Paris, France
[2] Equipe GALEN, INRIA Saclay - Île de France, France
[3] Section of Biomedical Image Analysis (SBIA), University of Pennsylvania, USA
[4] Computer Aided Medical Procedures (CAMP), Technische Universität München, Germany
aristeidis.sotiras@ecp.fr

Abstract. In this paper, we introduce a novel approach to bridge the gap between the landmark-based and the iconic-based voxel-wise registration methods. The registration problem is formulated with the use of Markov Random Field theory resulting in a discrete objective function consisting of thee parts. The first part of the energy accounts for the iconic-based volumetric registration problem while the second one for establishing geometrically meaningful correspondences by optimizing over a set of automatically generated mutually salient candidate pairs of points. The last part of the energy penalizes locally the difference between the dense deformation field due to the iconic-based registration and the implied displacements due to the obtained correspondences. Promising results in real MR brain data demonstrate the potentials of our approach.

1 Introduction

Image registration is a fundamental problem in medical image analysis. Due to its importance, great efforts have been made to tackle this problem resulting in numerous approaches. The existing methods fit mainly into two categories.

In the first class of methods, *geometric* (e.g. [1,2,3]), landmarks are detected and subsequently matched to establish correspondences between the images being registered. Such an approach exhibits strength and limitations. On one hand, if landmarks are appropriate determined, solving the registration problem is straightforward and the method is not sensitive to the initial conditions and can cope with important deformations. On the opposite side, the registration result is usually accurate in the vicinity of the interest points and its accuracy deteriorates away from them while often the extraction of landmarks is also problematic.

The second class of methods, *iconic* (e.g.[4,5,6,7]), takes advantage of the intensity information of all positions and tries to recover the deformation that optimizes a criterion based on it. Methods of this class exhibit globally better accuracy at the cost of greater computational effort. These approaches consider all points contributing equally to the objective function, thus discarding the importance of the salient points of the image. Furthermore, they are very sensitive to the initial conditions and often unable to deal with large deformations. Last but not least, their performance deteriorates when

T. Jiang et al. (Eds.): MICCAI 2010, Part II, LNCS 6362, pp. 676–683, 2010.

considering multi-modal image fusion where defining an appropriate similarity metric is far from being trivial, while at the same time the optimization of the objective function becomes more challenging.

During the last years, efforts have been made to bridge the two main classes of approaches by taking advantage of both complementing types of information, resulting in a *hybrid* approach (e.g.[8,9,10,11,12,13]). Among these methods, the way the two types of information are used varies widely. Most methods decompose the registration problem in two separate steps, each one exploiting information of one type. Typically, landmark information is used either to provide a coarse registration that is subsequently refined by using the intensity information [8] or more often, after having established point correspondences, use them in the objective function to ensure that the optimal deformation field will comply with them [10,11,12,13]. However, by considering geometric and iconic information in a non-coupled way, the solution of each subproblem (point correspondence, dense registration) cannot fully profit from the solution of the other. We refer to [9], where an objective function is proposed that combines an iconic-based dense field and geometric constraints and is optimized by alternating between three steps: estimate the dense deformation field, the point correspondences and regularize.

In this paper we couple the point correspondence and the dense registration problem into an unified objective function where the two problems are solved simultaneously in an one step optimization. We employ a Markov Random Field formulation towards introducing individual costs for the family of parameters and their interactions. Moreover, due to the discrete nature of the proposed objective function any intensity-based criterion can be used. To the best of our knowledge, only one other hybrid method can claim that [10], but it cannot guarantee the convergence as a ping-pong effect is possible between iterations. Moreover the proposed method is able to constrain the recovered dense deformation field to be diffeomorphic contrary to the rest of the hybrid methods. Last but not least, the influence of the landmarks is done in a local way and in respect to the deformation model used without the use of heuristics and any assumption on the number or the nature of the landmarks.

2 Iconic-Landmark Registration

Let us consider two images $I_1 : \Omega_1 \mapsto \mathbb{R}, I_2 : \Omega_2 \mapsto \mathbb{R}$, a set of points of interest $\mathcal{P}_1 \in \Omega_1$, and a set of potential candidates for the points $p_1 \in \mathcal{P}_1,\ \mathcal{P}_2 \in \Omega_2$ such that $|\mathcal{P}_2| > |\mathcal{P}_1|$. By $|\cdot|$ we denote the cardinality of the set. The aim of the algorithm is to estimate the deformation field $\mathcal{T} : \Omega_1 \mapsto \mathbb{R}^3$, such that an iconic criterion defined in the whole image domain is satisfied, and to recover the correspondences between the two different point sets such that the estimated solutions are consistent with each other.

A grid-based deformation model is going to be used, resulting in a decreased number of variables to be estimated. The dense deformation field is going to be given by interpolating the displacements of the grid points. Let us consider a deformation grid $G : [1, S_x] \times [1, S_y] \times [1, S_z]$ then,

$$\mathcal{T}(\mathbf{x}) = \mathbf{x} + \mathcal{D}(\mathbf{x}) \text{ where } \mathcal{D}(\mathbf{x}) = \sum_{p \in G} \eta(\|\mathbf{x} - \mathbf{p}\|)\mathbf{d_p}. \tag{1}$$

$\eta(\cdot)$ is a weighting function that measures the contribution of each control point to the displacement field $\mathcal{D}(\cdot)$. In the case of the cubic B-spline that are going to be used here, the weights are given by the cubic B-spline basis functions depending on the distance of the voxel from the control point. The specific deformation model allows diffeomorphic deformations to be guaranteed through the use of hard constraints [5].

The goal will be reached by coupling the dense deformation field estimation and the point correspondence problem in one with the use of the Markov Random Field (MRF) theory. The typical first-order MRF energy is of the form:

$$E_{MRF} = \sum_{p \in \mathcal{G}} V_p(l_p) + \sum_{p \in \mathcal{G}} \sum_{q \in \mathcal{N}(p)} V_{pq}(l_p, l_q) \tag{2}$$

where the first term (unary potentials) encodes the information stemming from the observed variables (intensity values) and typically acts as the data term of the energy. The second term (pairwise potentials) encodes relations between pairs of latent variables and typically acts as a regularizer. By l_p the label attributed to variable p is denoted.

2.1 Point Correspondence Problem

For the point correspondence part, the goal is to estimate which point $p_2 \in \mathcal{P}_2$ corresponds to each of the points $p_1 \in \mathcal{P}_1$. We are assuming that the true underlying anatomical correspondence is included in the set of potential candidates $\mathcal{P}_2$. The two point sets should capture the important geometric information of the two images in order to act as the additional constraints that will enhance the performance of the registration.

Any method for establishing candidate correspondences can be used. Herein, multi-scale and multi-orientation Gabor filters are used to locate points of interest in the image domain. Gabor filters are able to provide distinctive description for voxels belonging to different anatomical regions by capturing local texture information [14,15]. Local texture information reflects the underlying geometric and anatomical characteristics. Thus, points exhibiting a high response to Gabor filters are most likely placed in salient anatomical regions whose matching can be used to guide the registration process. In other words, the set $\mathcal{P}_1$ consists of points whose response to the Gabor filters is significant and that are distributed in space. Then, the set $\mathcal{P}_2$ of potential correspondences can be populated by taking for every $p_1 \in \mathcal{P}_1$, the top K candidate points in an appropriately defined sphere in terms of a similarity criterion that is based on the difference between D-dimensional Gabor attribute vectors $A(\cdot)$ weighted by the mutual saliency. The role of the mutual saliency, $ms(p_1, p_2) = \frac{mean_{n \in s_{in}}(sim(A(p_1), A(n)))}{mean_{n \in s_{out}}(sim(A(p_2), A(n)))}$ [15] (s_{in} and s_{out} are appropriately defined regions around the points and are adaptive to the scale from which Gabor attributes are extracted), is to narrow down the selection to candidate points that are mutually salient indicating matching reliability. The similarity is given by

$$sim(p_1, p_2) = \frac{1}{1 + \frac{1}{D}\|A(p_1) - A(p_2)\|^2}. \tag{3}$$

In a MRF framework, the point correspondence problem can be solved by minimizing an appropriately defined labeling energy. What we search is which label (or index

of candidate point) to attribute to each $p_1 \in \mathcal{P}_1$ to establish a correspondence. Thus, the label set is defined as $\mathcal{L}_{gm} = \{l^1, \cdots, l^K\}$, where the label assignment l_i^j corresponding the j-th potential candidate point to the i-th point/node. The optimal labeling $\mathbf{l}^\star = (l_1, \cdots, l_N)$ will minimize the discrete objective function. For that purpose, we are going to construct a graph $\mathcal{G}_{gm} = (\mathcal{V}_{gm}, \mathcal{E}_{gm})$ where the set of the nodes $\mathcal{V}_{gm}$ coincides with the point set $\mathcal{P}_1$ and each edge in $\mathcal{E}_{gm}$ encodes a geometric compatibility constraint.

The discrete objective function is of the type of Eq.2. The unary potentials will quantify the level of similarity between the landmark and its assigned candidate point.

$$V_p(l_p) = exp\left(-\frac{ms(p,p') \cdot sim(p,p')}{2\sigma^2}\right) \tag{4}$$

where p' is the point in $\mathcal{P}_2$ that is corresponded to p through a label assignment l_p and σ is a scaling parameter.

The regularization term will impose a geometric consistency on the established correspondences. What we would expect from the recovered pairs is that the distance between adjacent pairs should be preserved by their corresponded ones, thus avoiding having landmarks flipping positions. The pairwise potential is defined as:

$$V_{pq}(l_p, l_q) = \|(\mathbf{p} - \mathbf{q}) - (\mathbf{p}' - \mathbf{q}')\| \tag{5}$$

where in bold the physical position of the point is denoted. We consider that an affine registration step has preceded, as a consequence no normalization is needed.

2.2 Iconic Registration

For the estimation of the dense deformation field we follow the approach proposed in [6]. The reasons behind this choice lie in the fact that due to the discrete nature of the formulation a wide range of similarity measures can be used. Moreover, the method is computational efficient while producing precise results. For completeness reasons, the iconic registration method is going to be presented briefly in this section.

Given the deformation model, we aim at optimizing the displacements of the grid points. In the proposed discrete framework this is equivalent to assign a label to each grid node such that the displacement associated to it decreases the energy. For the iconic registration part, the label set $\mathcal{L}_{ic}$ is quantized version of the deformation space where each label l corresponds to a displacement $\mathbf{d}^l$. To impose the diffeomorphic property, the maximum displacement, to which a label is corresponded, is $0.4 \times \delta$ where δ is the grid spacing [5]. In order to solve the optimization problem, a regular graph $\mathcal{G}_{ig} = (\mathcal{V}_{ic}, \mathcal{E}_{ic})$ is going to be constructed. Its nodes coincide with the nodes of the deformation grid G and edges exist between neighboring nodes assuming a 6-connectivity scheme.

The unary potentials are defined as follows:

$$V_p(l_p) = \int \hat{\eta}(\|\mathbf{x} - \mathbf{p}\|)\rho(I_1(\mathbf{x} + \mathbf{d}^{l_p}), I_2(\mathbf{x}))d\mathbf{x} \tag{6}$$

The data term is based on an iconic similarity measure $\rho(\cdot)$ and $\hat{\eta}(\cdot)$ is a function that determines how much a voxel $\mathbf{x}$ influences a node p. It is defined as

$$\hat{\eta}(\|\mathbf{x}-\mathbf{p}\|) = \frac{\eta(\|\mathbf{x}-\mathbf{p}\|)}{\int_{\Omega}\eta(\|\mathbf{y}-\mathbf{p}\|)d\mathbf{y}} \text{ or } \hat{\eta}(\|\mathbf{x}-\mathbf{p}\|) = \begin{cases} 1, & \text{if } \eta(\|\mathbf{x}-\mathbf{p}\|) > 0, \\ 0, & \text{else.} \end{cases} \tag{7}$$

for the case of voxel-wise and more sophisticated statistical criteria respectively. The regularization term in the simplest case can be a vector difference between the displacements that are encoded by the two different labels normalized by the difference of the control points,

$$V_{pq}(l_p, l_q) = \frac{\|\mathbf{d}^{l_p} - \mathbf{d}^{l_q}\|}{\|\mathbf{p}-\mathbf{q}\|} \tag{8}$$

2.3 Simultaneous Geometric - Iconic Registration

In order to tackle both problems at the same time, a new graph $\mathcal{G} = (\mathcal{V}, \mathcal{E})$ should be considered. The node system of the new graph is simply the union of the nodes of the subproblems $\mathcal{V} = \mathcal{V}_{ic} \cup \mathcal{V}_{gm}$. The edge system of the graph will comprise of the edges of each subproblem and appropriate edges that will connect the two graphs and will encode the consistency between the solutions of the two subproblems $\mathcal{E} = \mathcal{E}_{ic} \cup \mathcal{E}_{gm} \cup \mathcal{E}_{cn}$.

The unary potentials and the pairwise potentials will be the same as the ones previously detailed except from the ones that correspond to the new edges and have yet to be detailed. In order to impose consistency upon the solutions of the two subproblems, the difference between the displacement field due to the grid-based deformation model and the displacement implied by the recovered correspondence should be minimal at the landmark position. Given a cubic B-spline FFD deformation model and considering, without loss of generality, only one landmark, then

$$0 = \|\mathcal{D}(\mathbf{x}_*) - (\mathbf{p}'_* - \mathbf{p}_*)\| = \|\sum_{i=1}^{M}\beta_i(\mathbf{x}_*)\mathbf{d}_{p_i} - \mathbf{d}_{p_*}\| =$$
$$\|\sum_{i=1}^{M}\beta_i(\mathbf{x}_*)\mathbf{d}_{p_i} - \sum_{i=1}^{M}\beta_i(\mathbf{x}_*)\mathbf{d}_{p_*}\| \leq \sum_{i=1}^{M}\beta_i(\mathbf{x}_*)\|\mathbf{d}_{p_i} - \mathbf{d}_{p_*}\| \tag{9}$$

where the displacement of the voxel $\mathbf{x}_*$ is $\mathbf{d}_{p_*} = \mathbf{p}'_* - \mathbf{p}_*$ and the properties of the cubic B-spline, $\sum_i^M \beta_i(\cdot) = 1,\ \beta_i(\cdot) \geq 0$, and the triangular inequality were used. $M = 4 \times 4 \times 4$, the number of the grid nodes that control the displacement of a voxel.

The previous relation (Eq.9) can be modeled by adding edges between the nodes of the irregular grid $\mathcal{V}_{gm}$ and those nodes of the regular grid $\mathcal{V}_{ic}$ that control the displacement of the position in which the landmark is placed. The pairwise potentials are given by the following equation

$$V_{pq}(l_p, l_q) = w\|\mathbf{d}^{l_q} - (\mathbf{p}' - \mathbf{p})\|. \tag{10}$$

p, p' and $\mathbf{d}^{l_q}$ are defined as previous. w is a weight based on the cubic B-spline basis as a function of the distance of the landmark from the control point q. This formulation

results in minimizing an upper bound of the energy while permitting us to model the problem by pairwise relations between the latent variable and thus allowing for the use of any standard MRF optimization technique.

3 Experimental Validation

3.1 MRF Optimization

In order to optimize the resulting MRF problem, the convergent Tree-Reweighted (TRW) Message Passing algorithm was used [16]. The TRW algorithm aims to address the MRF optimization problem by tackling the simpler dual of its Linear Programming (LP) relaxation. Any solution of this problem is a lower bound to the energy of the original problem. Thus, the TRW algorithm aims to maximize the bound and thus reach a solution. TRW is known to have a state of the art performance among the various discrete optimization methods and has proven its applicability in various tasks in the fields of computer vision and medical imaging.

3.2 Experimental Results

To validate the proposed method, a data set of 11 $T1$-weighted brain images of different subjects was used. The resolution of the images is $256 \times 256 \times 181$ with an isotropic voxel spacing of $1mm$. The volumes were manually annotated into 11 classes (background, cerebrospinal fluid, white matter, gray matter, fat, muscle, muscle/skin, skull, around fat, dura matter and bone marrow). The Sum of Absolute Differences (SAD) was used as iconic similarity criterion.

To visually assess the quality of the registration, a template image is chosen and all the rest are registered to it. Then the mean image, its difference with the template as well as the standard deviation image are calculated for the images before and after the registration (Fig.1). The blur mean image and the great values for the standard deviation before registration depict the difficulty of the registration task. On the bottom row, the mean image has become sharper indicating that the images have been spatially normalized. The values of the standard deviation have decreased especially in the area of the ventricles. The results of the registration can be also seen when comparing the two difference images and noting that the difference image (c2) is darker than (c1).

To further quantify the performance of the algorithm, we performed all possible 110 pair-wise registrations and the provided voxel-wise manual segmentations are used to measure the accuracy of the proposed method. We select each one of the images as target and register the rest to it. The obtained deformation fields are then used to warp the segmentations. Finally, we compare the deformed segmentations with the manual ones by calculating the DICE overlap measure, its sensitivity and specificity. The results are presented graphically in Fig.2 in the form of box plots. When comparing the obtained results to the initial DICE coefficients, it becomes evident the impact of the registration. Moreover, we compare the proposed method with the one that only uses the iconic information to show the added value of the use of the landmark information. The iconic registration is performed by discarding the landmark information in the proposed framework. In a similar way, DICE, sensitivity and specificity are computed for

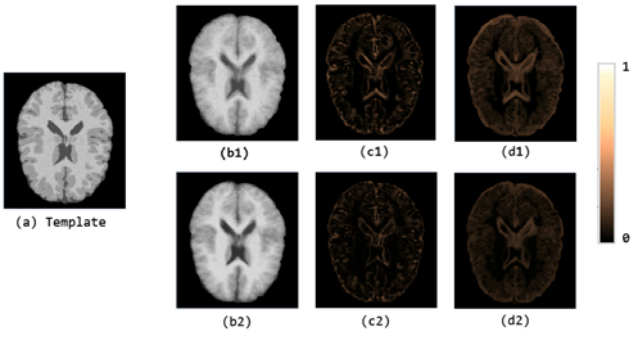

Fig. 1. (a)Template image. Top row: the mean image, the difference between the template and the mean image, the standard deviation image for the data-set before registration. Bottom row, the respective images for the group after registration.

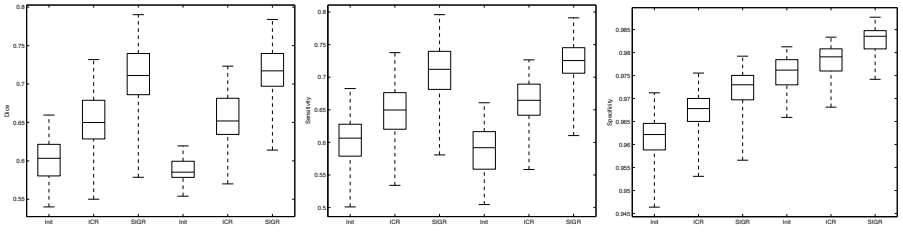

Fig. 2. From left to right, DICE coefficients, sensitivity and specificity for gray matter and white matter segmentations initially (Init) and after applying the iconic registration method (ICR) and the simultaneous geometric-iconic registration method (SIGR) respectively. The first three results are for the gray matter while the next ones for the white matter.

the iconic registration and are presented in Fig.2. From the comparison of the DICE values, it can be concluded that the addition of the landmark information has ameliorated the registration result as the DICE values for the geometric - iconic registration are greater than the values of the iconic one. Moreover, it can be concluded that the addition of the landmark information has rendered the registration less sensitive to the initial conditions. This can be justified by the difference between the worst case results produced by both methods.

4 Discussion

In this paper we have proposed a novel approach to couple geometric (landmark) and iconic (voxel-wise) registration. The proposed method is, to the best of our knowledge, the first to propose an one-shot optimization on the joint parameter space, and therefore inherits ability to capture large deformations, independence with respect to the initial conditions, smooth and continuous diffeomorphic dense field, while being able to account for various similarity metrics and arbitrary number and position of landmarks. Promising results demonstrate the potentials of this elegant formulation.

The bias introduced from the landmark extraction process is an important limitation of the method. Such a limitation can be dealt with the use of the notion of missing correspondences. This is something that we are willing to address in the near future. The use of higher order model interactions between graph nodes is also interesting, since it could make the framework rigid or similarity invariant. Last but not least, the encouraging results that were obtained in the intra-modality case suggest that the application of the proposed method in the problem of multi-modal image fusion could be of significant interest.

References

1. Joshi, S., Miller, M.: Landmark matching via large deformation diffeomorphisms. In: IEEE TIP (2000)
2. Shen, D., Davatzikos, C.: Hammer: hierarchical attribute matching mechanism for elastic registration. In: IEEE TMI (2002)
3. Chui, H., Rangarajan, A.: A new point matching algorithm for non-rigid registration. In: CVIU (2003)
4. Beg, M.F., Miller, M.I., Trouvé, A., Younes, L.: Computing large deformation metric mappings via geodesic flows of diffeomorphisms. CVIU (2005)
5. Rueckert, D., Aljabar, P., Heckemann, R.A., Hajnal, J.V., Hammers, A.: Diffeomorphic registration using b-splines. In: Larsen, R., Nielsen, M., Sporring, J. (eds.) MICCAI 2006. LNCS, vol. 4191, pp. 702–709. Springer, Heidelberg (2006)
6. Glocker, B., Komodakis, N., Tziritas, G., Navab, N., Paragios, N.: Dense image registration through mrfs and efficient linear programming. In: MedIA (2008)
7. Vercauteren, T., Pennec, X., Perchant, A., Ayache, N.: Diffeomorphic demons: Efficient non-parametric image registration. NeuroImage (2009)
8. Johnson, H., Christensen, G.: Consistent landmark and intensity-based image registration. In: IEEE TMI (2002)
9. Cachier, P., Mangin, J.F., Pennec, X., Riviere, D., Papadopoulos-Orfanos, D., Règis, J.: Multisubject non-rigid registration of brain MRI using intensity and geometric features. In: Niessen, W.J., Viergever, M.A. (eds.) MICCAI 2001. LNCS, vol. 2208, p. 734. Springer, Heidelberg (2001)
10. Azar, A., Xu, C., Pennec, X., Ayache, N.: An interactive hybrid non-rigid registration framework for 3d medical images. In: IEEE ISBI (2006)
11. Biesdorf, A., Wörz, S., Kaiser, H.J., Stippich, C., Rohr, K.: Hybrid spline-based multimodal registration using local measures for joint entropy and mutual information. In: Yang, G.-Z., Hawkes, D., Rueckert, D., Noble, A., Taylor, C. (eds.) MICCAI 2009. LNCS, vol. 5761, pp. 607–615. Springer, Heidelberg (2009)
12. Hellier, P., Barillot, C.: Coupling dense and landmark-based approaches for nonrigid registration. In: IEEE TMI (2003)
13. Papademetris, X., Jakowski, A.P., Schultz, R.T., Staib, L.H., Duncan, J.S.: Integrated intensity and point-feature nonrigid registration. In: Barillot, C., Haynor, D.R., Hellier, P. (eds.) MICCAI 2004. LNCS, vol. 3216, pp. 763–770. Springer, Heidelberg (2004)
14. Zhan, Y., Shen, D.: Deformable segmentation of 3-d ultrasound prostate images using statistical texture matching method. In: IEEE TMI (2006)
15. Ou, Y., Davatzikos, C.: Dramms: Deformable registration via attribute matching and mutual-saliency weighting. In: Prince, J.L., Pham, D.L., Myers, K.J. (eds.) IPMI 2009. LNCS, vol. 5636, pp. 50–62. Springer, Heidelberg (2009)
16. Kolmogorov, V.: Convergent tree-reweighted message passing for energy minimization. IEEE PAMI 28 (2006)